SUPPORTING INFORMATION

Highly sensitive SERS quantification of organophosphorous chemical warfare agents: a major step towards the real time sensing in the gas phase

Marta Lafuente,[a] Ismael Pellejero,[a,b] Víctor Sebastián,[a,c] Miguel A. Urbiztondo,[d] Reyes Mallada,[a,c] M. Pilar Pina*,[a,c] Jesús Santamaría*,[a,c]

[a]Nanoscience Institute of Aragon, University of Zaragoza, Department of Chemical & Environmental Engineering, Edif. I+D+i, Campus Rio Ebro, C/Mariano Esquillor, s/n, 50018 Zaragoza, Spain.
[b]Institute for Advanced Materials, Public University of Navarre, Edif. Jerónimo de Ayanz, Campus Arrosadia, s/n, 31006 Pamplona-Iruña, Spain.
[c]Networking Research Center on Bioengineering, Biomaterials and Nanomedicine, CIBER-BBN, 28029 Madrid, Spain.
[d]Centro Universitario de la Defensa de Zaragoza, 50090 Zaragoza, Spain.
* Corresponding authors: mapina@unizar.es (M.P.P.) and jesus.santamaria@unizar.es (J.S.)

Figure captions:

Table S1. Enhancement factor calculated using different methods.

Figure S1. Au@citrate particle size distribution from DLS measurements at room temperature.

Figure S2. Au@citrate coatings: PDDA concentration (A) and (D) and spin-coating rate (B) and (E) dependence. SEM images of SERS substrates prepared without PDDA as linker (C)

Figure S3. Evaluation of the thickness of the PDDA layer by AFM.

Figure S4. SEM image (A) and AFM image (B) of SiO2/Si chip with evaporated thin layer of 9 nm of gold.

Figure S5. Chemical structure of sarin and its simulant. Image key: C, grey; H, white; O, red; P, purple; F, blue.

Figure S6. Temporal evolution of DMMP SERS intensity (peak at 715cm^{-1}) monitored on AuNP@citrate substrate.

Figure S7. Raman spectrum of DMMP solution (>97% purity) and band assignment.

Figure S8. SEM images of high-density gold monolayers before (left) and after (right) the O_2 plasma treatment defined for citrate layer removal. The absence of Au sintering or of other substantial changes in the ordering of Au NPs in the monolayer can be observed.

Figure S9. Estimation of the number of DMMP vapor molecules confined in the scattering volume.

Particle Size Distribution of Au@citrate NPs evaluated by DLS

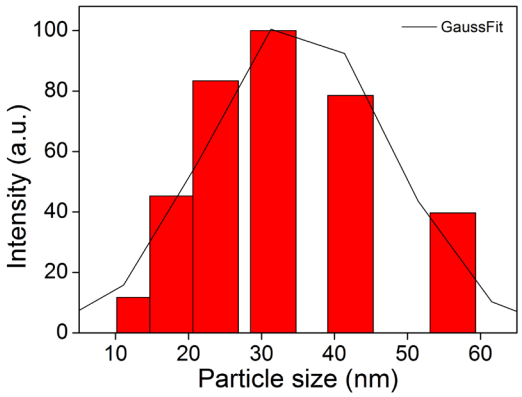

Figure S1. Au@citrate particle size distribution from DLS measurements at room temperature.

Preparation of high density Au@citrate coatings by electrostatic interactions:
Influence of PDDA concentration and spinning rate on the assembly of Au@citrate NPs on SiO_2/Si chips.

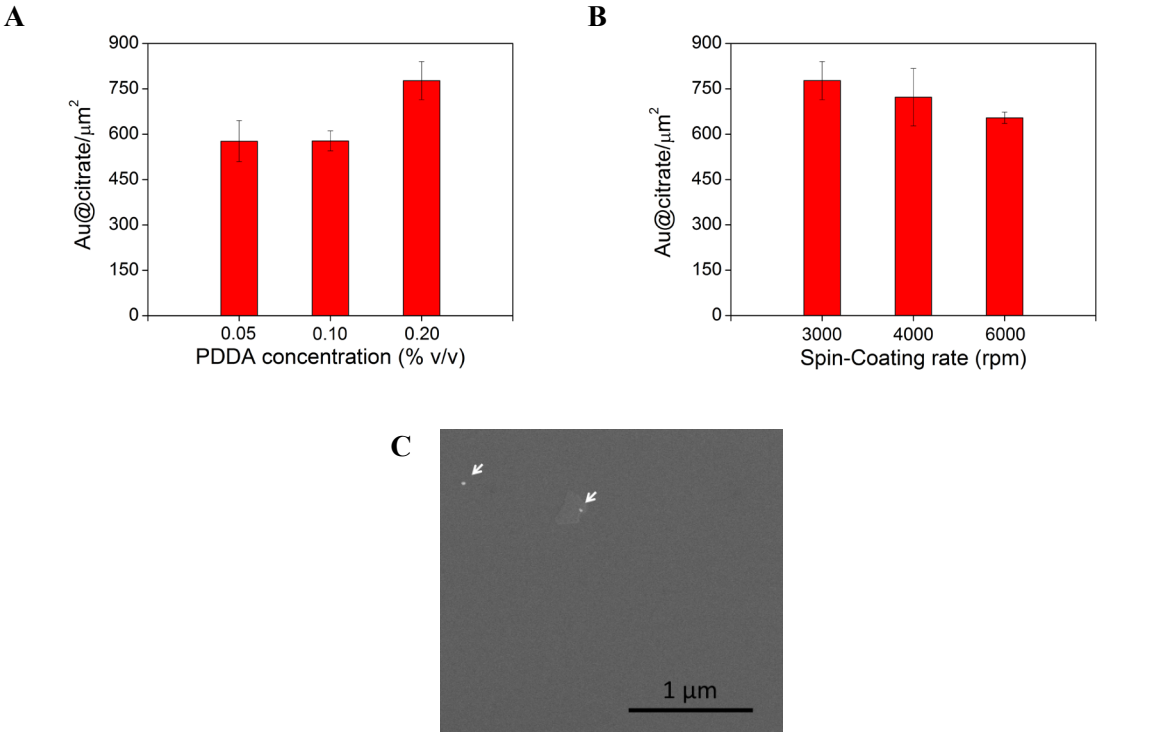

(D) Influence of the PDDA concentration (3000 rpm - 60s)

0.05 % v/v	0.1 % v/v	0.2 % v/v

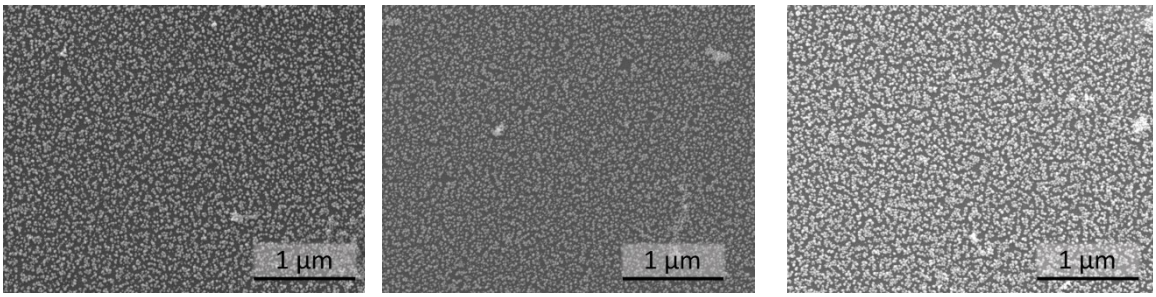

(E) Influence of the spin-coating rate (0.2 % v/v PDDA solution, 60 s spinning)

3000 rpm	4000 rpm	6000 rpm

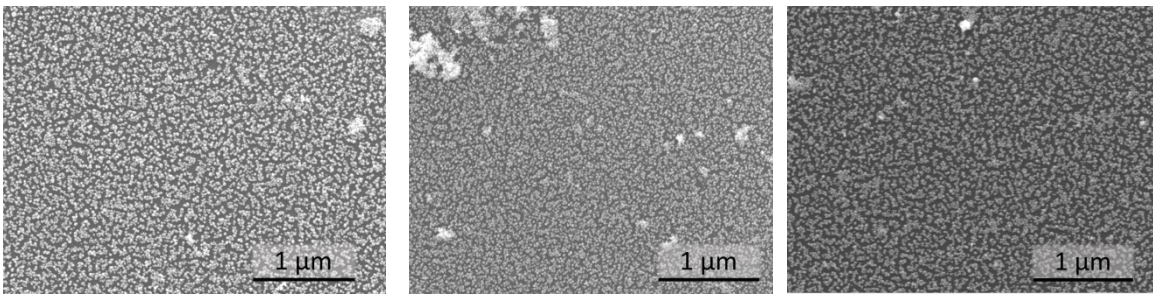

Figure S2. Au@citrate coatings: PDDA concentration (A) and (D) and spin-coating rate (B) and (E) dependence. SEM images of SERS substrates prepared without PDDA as linker (C).

Thickness of the PDDA layer on SiO_2/Si chips obtained at 3000 rpm of 0.2% v/v in water solution.

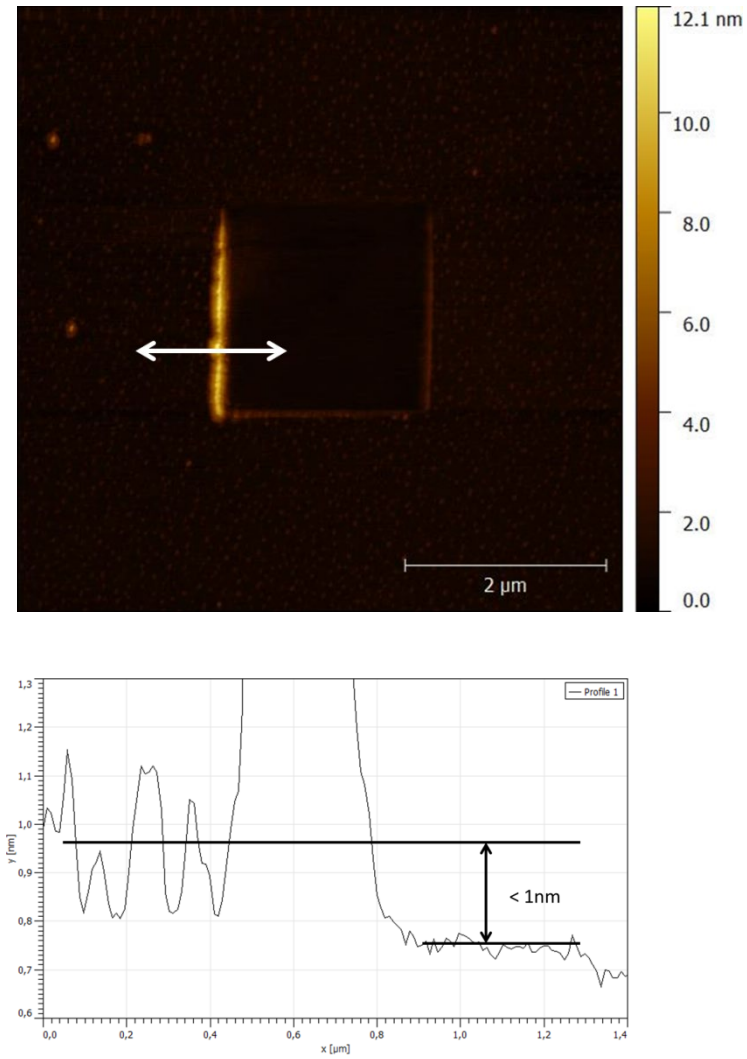

Figure S3. Evaluation of the thickness of the PDDA layer by AFM.

- Experimental procedure for the evaluation of PDDA thickness by AFM:

The PDDA layer (0.2%v/v, 3000 rpm, rinsed in water and dried) was peeled using the AFM tip (2x2 µm; force, 1 µN; 256 lines per area; scan rate, 1HZ) and then, the topography of the same area was measured by AFM (area 6x6 µm, 200 nN). Preliminary studies demonstrated that 1 µN did not scratch the SiO_2/Si surface.

Enhancement Factor Estimation according to different approaches found in the literature

- SEM and AFM analysis of the Reference Substrate

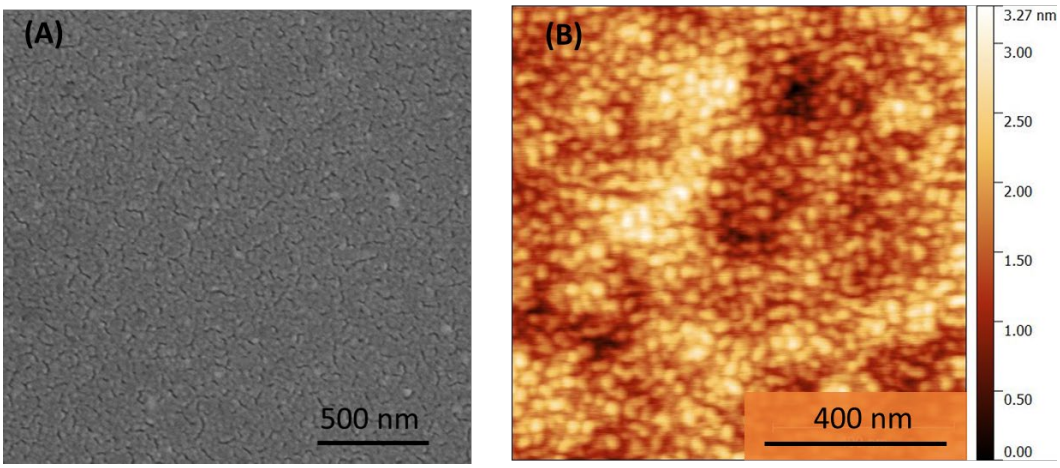

Figure S4. SEM image (A) and AFM image (B) of SiO_2/Si chip with evaporated thin layer of 9 nm of gold.

Table S1. SERS Substrate Enhancement factor values calculated from different approaches.

	Method 1 [1-3]	**Method 2** [4]	**Method 3**
$\mathbf{I_{ref}}$	6.5 cts/s (1 liquid drop, 1mM)	335 cts/s (powder)	19.4 cts/s (2 dried droplets, 1 µM)
$\mathbf{N_{ref}}$	3.41 x 10^7 molecules	1.35 x 10^9 molecules	6.00 x 10^5 molecules
$\mathbf{I_{SERS}}$	11012 cts/s (1 dried droplet, 1µM)	11012 cts/s (1 dried droplet, 1µM)	11012 cts/s (1 dried droplet, 1µM)
$\mathbf{N_{SERS}}$	3.00 x 10^5 molecules	5.65 x 10^5 molecules	3.00 x 10^5 molecules
EF	**1.93 x 10^5**	**7.85 x 10^4**	**1.13 x 10^3**

- Method 1 (used in this article):

The R6G Raman spectrum was measured in the centre of the liquid droplet (2µL in volume) of aqueous solution of R6G 10^{-3} M over the reference substrate (Au film 9 nm thick prepared by electron beam evaporation on Si chip).

$$N_{ref,method\ 1} = 6.023 \cdot 10^{23} \frac{molecules}{mol} \times (R6Gconcentration) \times (Interaction\ volume)$$

The laser interaction/probe volume was determined by placing the reference substrate in the focus plane and then moving the substrate out of the focus plane in increments of 1 µm. Thus the interaction volume using a 50X objective and a laser power of 1mW was measured to be 56.5 μm^3.

The R6G SERS spectrum on the SERS substrate was measured in the centre of the liquid droplet (2µL in volume) of aqueous solution of R6G 10^{-6} M once dried.

$$N_{SERS,method\ 1} = \frac{(R6G\ molecules\ in\ the\ droplet) \times (area\ of\ laser\ spot)}{surface\ area\ of\ the\ dried\ droplet}$$

- Method 2:

The reference R6G was measured using R6G powder (M_{R6G} = 479 g/mol; ρ_{R6G} = 0.79 g/cm^3) onto the reference substrate (Au film 9 nm thick prepared by electron beam evaporation on Si chip). The calculation of Nref was based on the laser penetration depth[5] (1.2 µm), the area of laser spot (1.13 µm^2) and density and molar mass of R6G.

$$N_{ref,method\ 2} = \frac{6.023 \cdot 10^{23} \frac{molecules}{mol} \times \rho_{R6G} \times (laser\ spot\ \times laser\ penetration\ depth)}{M_{R6G}}$$

The R6G SERS spectrum on the SERS substrate was measured in the centre of the liquid droplet (2µL in volume) of aqueous solution of R6G 10^{-6} M once dried. The number of molecules inside the effective laser spot was estimated by assuming a monolayer of R6G (cross section 2 nm^2) all over the substrate. A packing density of 5 x 10^5 R6G molecules/µm^2 was used for this calculation. With a laser spot size with diameter 1.2 µm, the surface area probed by the laser was 1.13 µm^2, and the number of R6G molecules in the laser spot (N_{SERS}) is 5.65 x 10^5 molecules.

$$N_{SERS,method\ 2} = \frac{area\ of\ laser\ spot}{area\ of\ single\ R6G\ molecule}$$

- Method 3:

Following this approach, both substrates were evaluated almost under identical conditions. As long as the same experimental conditions are kept, the results are directly comparable. The R6G SERS spectrum on the reference (I_{ref}) and SERS (I_{SERS}) substrates was measured in the centre of the liquid droplet (2µL in volume) of aqueous solution of R6G 10^{-6} M once dried. I_{ref} and I_{SERS} were normalized by the number of droplets, i.e 2 drops for reference substrate and 1 for SERS substrate. Similar wetting properties were assumed for both substrates.

Chemical structure of Sarin and DMMP simulant

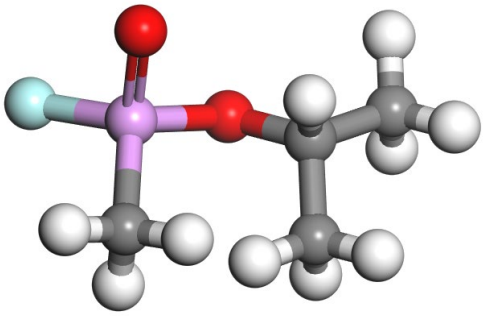

Sarin
(CAS number: 107-44-8)

2-(fluoro-methyl-phosphoryl)oxypropane

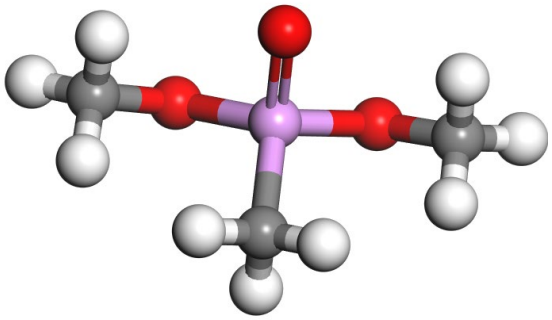

DMMP Simulant
(CAS number: 756-79-6)

Dimethyl methylphosphonate

Figure S5. Similarities among Sarin gas and DMMP, as simulant. Image key: C, grey; H, white; O, red; P, purple; F, blue.

Monitoring of the SERS signal upon DMMP dosing to the home-made gas chamber

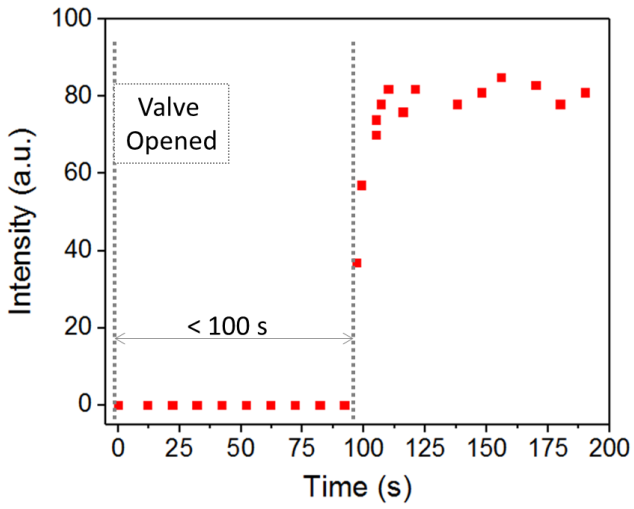

Figure S6. Temporal evolution of DMMP SERS intensity (peak at 715cm^{-1}) monitored on AuNP@citrate substrate. Experimental conditions: 2.5 ppmV of DMMP, 10 cm^3/min, excitation power 1 mW, integration time 0.5 s.

Normal Raman vibrational fingerprint of DMMP

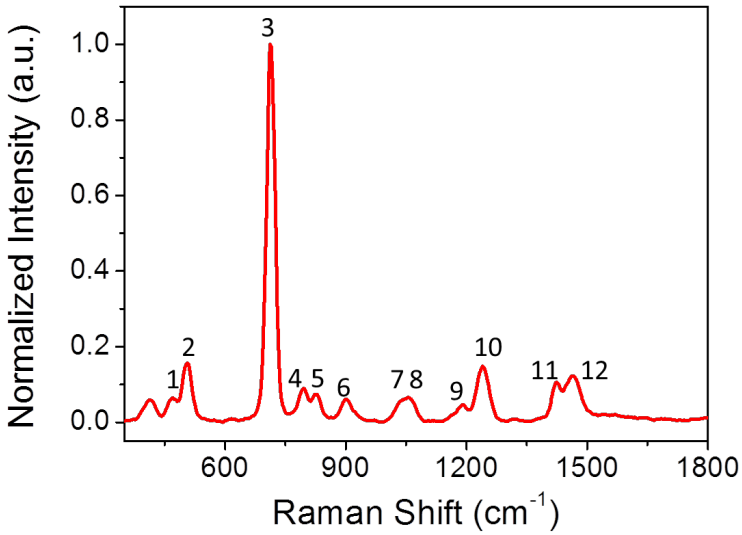

Band no.	Band Position (cm^{-1})	Tentative Assignment
1	466	Bending $POCH_3$
2	504	POC
3	718	Stretching PC
4	794	Bending PO_2
5	825	Bending PO_2
6	903	Rocking CH_3O
7	1039	Stretching C-O
8	1062	Stretching C-O
9	1183	Bending CH_3
10	1240	Stretching P=O Bending CH_3
11	1419	Bending CH_3
12	1424	Bending CH_3P

Figure S7. Raman spectrum of DMMP solution (>97% purity) and band assignment.

Optimization of the O_2 plasma conditions for citrate removal without Au sintering

Before O_2 plasma treatment	After mild O_2 plasma treatment
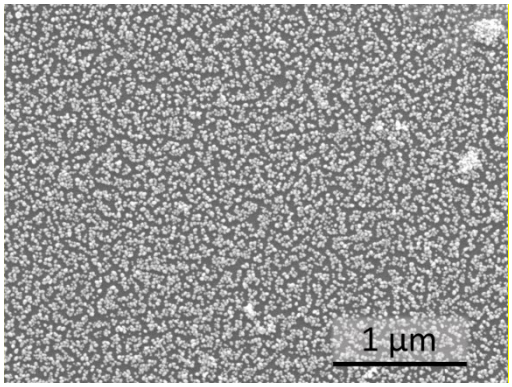	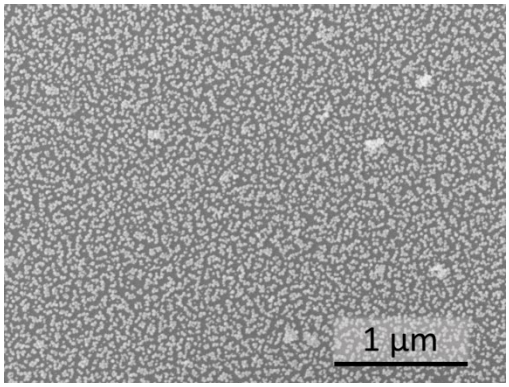

Figure S8. SEM images of high-density gold monolayers before (left) and after (right) the O_2 plasma treatment defined for citrate layer removal. The absence of Au sintering or of other substantial changes in the ordering of Au NPs in the monolayer can be observed.

Comparative SERS performance with commercial Au coated SERStrates® supplied by SILMECO

A)

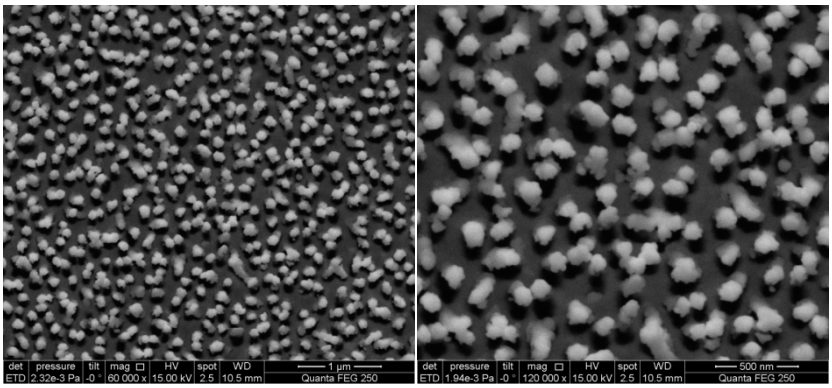

B)

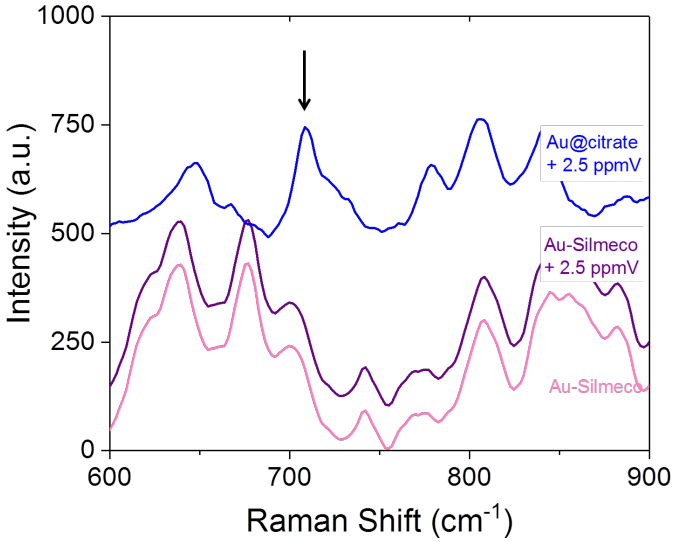

Figure S9. A) SEM images of the Au coated SERStrate® substrates supplied by SILMECO with a density of flexible Si nanopillars of 21 μm^{-2}. B)Comparative SERS spectrum of DMMP in gas phase (2.5 ppmV) obtained with the high-density Au@citrate monolayers onto SiO2/Si chip (blue) prepared in this work and with a commercial Au-Silmeco substrate (dark pink) after pillar leaning. The spectrum of Au-Silmeco in pure N2 gas phase (pink) is also included as reference. Experimental conditions: excitation power 5 mW, integration time 1 s. Arrow point indicates the main vibrational mode of DMMP.

Role of the citrate layer on DMMP detection:

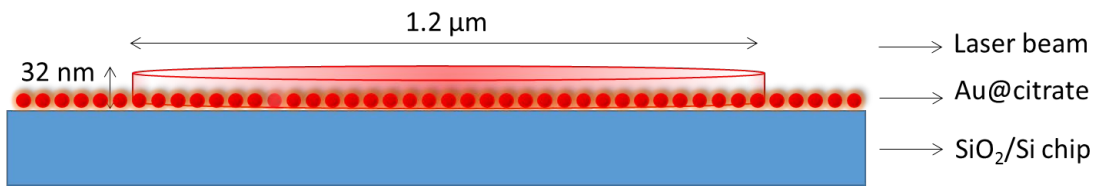

Figure S10. Estimation of the number of DMMP vapor molecules confined in the effective scattering volume.

DMMP concentration = 2.5 ppmV
k = Molar density (at 298 K, 1 atm)= 1 mol /24448 cm^3
NA = Nº Avogadro = 6.023×10^{23} molecules/mol

$$DMMP\ concentration \cdot Effective\ Scattering\ Volume \cdot k \cdot NA =$$

$$= 2.5 \cdot 10^{-6}\ \frac{cm^3 DMMP}{cm^3 gas} \cdot \left(\pi \cdot \left(\frac{1.2 \cdot 10^{-4} cm}{2} \right)^2 \cdot (32 \cdot 10^{-7} cm) \right) \cdot \frac{1\ mol\ DMMP}{24448\ cm^3} \cdot 6.023 \cdot 10^{23} \frac{molecules}{mol}$$

$$< 3\ DMMP\ molecules$$

Reference:

(1) Rodríguez-Lorenzo, L.; Alvarez-Puebla, R. A.; Pastoriza-Santos, I.; Mazzucco, S.; Stéphan, O.; Kociak, M.; Liz-Marzán, L. M.; García de Abajo, F. J. Zeptomol Detection through Controlled Ultrasensitive Surface Enhanced Raman Scattering. *J. Am. Chem. Soc.* **2009**, *131*, 4616-4618.

(2) McFarland, A. D.; Young, M. A.; Dieringer, J. A.; Van Duyne, R. P. Wavelength Scanned Surface Enhanced Raman Excitation Spectroscopy. *J. Phys. Chem. B* **2005**, *109*, 11279-11285.

(3) Schmidt, M. S.; Hübner, J.; Boisen, A. Large Area Fabrication of Leaning Silicon Nanopillars for Surface Enhanced Raman Spectroscopy. *Adv. Mater.* **2012**, *24*, OP11–OP18.

(4) Chen, Y.; Zhang, Y.; Pan, F.; Liu, J.; Wang, K.; Zhang, C.; Cheng, S.; Lu, L.; Zhang, W.; Zhang, Z.; Zhi, X.; Zhang, Q.; Alfranca, G.; de la Fuente, J.M.; Chen, D.; Cui, D. Breath Analysis Based on Surface Enhanced Raman Scattering Sensors Distinguishes Early and Advanced Gastric Cancer Patients from Healthy Persons. *ACS Nano* **2016**, *10*, 8169-8179.

(5) Álvarez-Puebla, R. A. Effects of the Excitation Wavelength on the SERS Spectrum. *J. Phys. Chem. Lett.* **2012**, *3*, 857-866.